



Contents lists available at ScienceDirect

Solid-State Electronics

journal homepage: [www.elsevier.com/locate/sse](http://www.elsevier.com/locate/sse)

## Thermoelectric generators from $\text{SiO}_2/\text{SiO}_2 + \text{Ge}$ nanolayer thin films modified by MeV Si ions

S. Budak<sup>a,\*</sup>, E. Gulduren<sup>b</sup>, B. Allen<sup>a</sup>, J. Cole<sup>a</sup>, J. Lassiter<sup>c</sup>, T. Colon<sup>d</sup>, C. Muntele<sup>e</sup>, M.A. Alim<sup>a</sup>, S. Bhattacharjee<sup>f</sup>, R.B. Johnson<sup>d</sup>

<sup>a</sup> Department of Electrical Engineering & Computer Science, Alabama A&M University, Huntsville, AL, USA

<sup>b</sup> Department of Physics, University of Alabama in Huntsville, Huntsville, AL, USA

<sup>c</sup> Materials Research Laboratory, Alabama A&M University, Huntsville, AL, USA

<sup>d</sup> Department of Physics, Alabama A&M University, Huntsville, AL, USA

<sup>e</sup> Cygnus Scientific Services, Huntsville, AL 35815, USA

<sup>f</sup> Department of Mechanical and Civil Engineering, Alabama A&M University, Huntsville, AL, USA

### ARTICLE INFO

#### Article history:

Received 10 April 2014

Received in revised form 14 August 2014

Accepted 16 August 2014

Available online xxxx

The review of this paper was arranged by Prof. S. Cristoloveanu

#### Keywords:

Ion bombardment

Thermoelectric properties

Multi-nanolayers

Impedance analysis

### ABSTRACT

We prepared thermoelectric generator devices from 100 alternating layers of  $\text{SiO}_2/\text{SiO}_2 + \text{Ge}$  superlattice thin films using Magnetron DC/RF Sputtering. Rutherford Backscattering Spectrometry (RBS) and RUMP simulation software package were used to determine the proportions of Si and Ge in the grown multi-layer films and the thickness of the grown multi-layer films. 5 MeV Si ion bombardments were performed using the AAMU-Pelletron ion beam accelerator, to form quantum clusters in the multi-layer superlattice thin films, in order to tailor the thermoelectrical and optical properties. We characterized the fabricated thermoelectric devices using cross-plane Seebeck coefficient, van der Pauw resistivity, mobility, density (carrier concentration), Hall Effect coefficient, Raman, Fluorescence, Photoluminescence, Atomic Force Microscopy (AFM) and Impedance analyzing measurements. Some suitable high energy ion fluences and thermal annealings caused some remarkable thermoelectrical and optical changes in the fabricated multilayer thin film systems.

© 2014 Elsevier Ltd. All rights reserved.

### 1. Introduction

The requirement of clean energy and the related technological developments lead to extensive research into renewable energy resources. One of the promising clean energy sources is the thermoelectric power generators. Since these devices do not have moving parts, the operation and maintenance of thermoelectric power generator is easy and less costly [1]. Although thermoelectrics (TE) as a physical phenomenon has been known for 190 years, there are still no well-established, widespread TE applications for power generation in households or industry. Intensive research among the materials aimed for improving the thermoelectric performance and providing benefits for both cost and environment benefits has recently been stimulated by advances in nano-structuring of semi-conducting materials [2]. Due to the advantages of thermoelectric oxides including their high-temperature thermal stability under conditions that oxidize semiconductor alloys, sufficient source supply, and environment friendly compositions, oxide

thermoelectric materials have been recognized as promising candidates for applications in high-temperature thermoelectric power generation [3]. Oxide materials are potential candidates for a wide range of high temperature applications due to their high chemical stability and the absence of harmful elements in their compositions. On the other hand, improving thermoelectric performance of n-type oxides has been under intensive investigation because of their inferior properties compared to p-type materials [4]. Thermoelectric generators present potential applications in the conversion of low level thermal energy into electrical power. Especially in the case of waste heat recovery, it is unnecessary to consider the cost of the thermal energy input, and there are additional advantages, such as energy saving and emission reduction. Thus, the low efficiency problem is no longer the most important issue that people have to take into account [5]. Advances in nanotechnology make the production of mechanical structures and thermodynamic systems in nano-scale possible. For example, by introducing quantum tunneling, nanowires, etc., nano-scaled thermionic devices could overcome the defects of conventional devices only working only at high temperatures and obtain higher efficiency and coefficient of performance than conventional devices [6]. Significant

\* Corresponding author. Tel.: +1 256 372 5894; fax: +1 256 372 5855.

E-mail address: [satilmis.budak@aamu.edu](mailto:satilmis.budak@aamu.edu) (S. Budak).

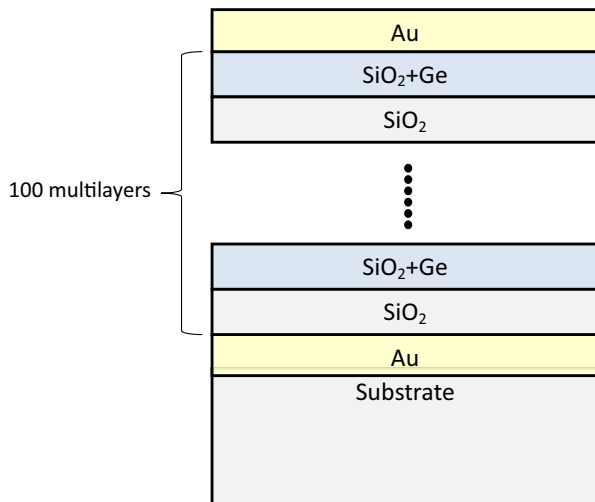


Fig. 1. Cross-plane geometry of the prepared multilayer thin films.

progress has been performed in recent years and it indicates that low-dimensional materials have higher thermoelectric conversion efficiency. Thermoelectric thin film is one of the important low-dimensional thermoelectric materials due to its stronger quantum confinement compared with that of their bulk materials, a potentially more favorable carrier scattering mechanism, and a much lower lattice thermal conductivity [7]. TE includes the Seebeck, Peltier, and Thomson effects. TE is also associated with other effects, such as Joulean and Fourier effects. TE generation has primarily been directed toward increasing the material figure of merit ( $ZT$ ), which is the standard measure of the TE performance of a material [8]. The figure of merit is defined by  $ZT = S^2 \sigma T / K$ , where  $S$  is the Seebeck coefficient,  $\sigma$  is the electrical conductivity,  $T$  is the absolute temperature, and  $K$  is the thermal conductivity.  $ZT$  can be increased by increasing  $S$ , by increasing  $\sigma$ , or by decreasing  $K$ . In order to compete with conventional refrigerators, a  $ZT$  of 3 is required. Due to their limited energy conversion efficiencies (i.e.  $ZT$  is  $\sim 1$ ), thermoelectric devices currently have a rather narrow set of applications. However, there is a reinvigorated interest in the field of thermoelectrics due to classical and quantum mechanical size

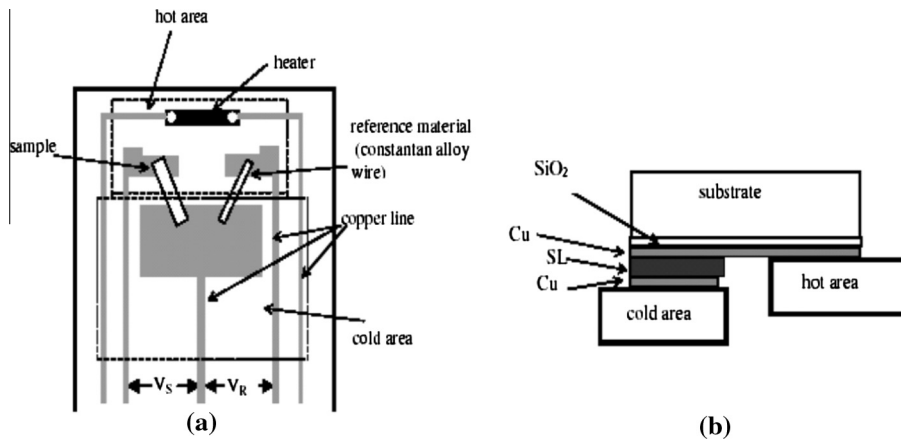


Fig. 2. The geometry for the Seebeck coefficient measurement.

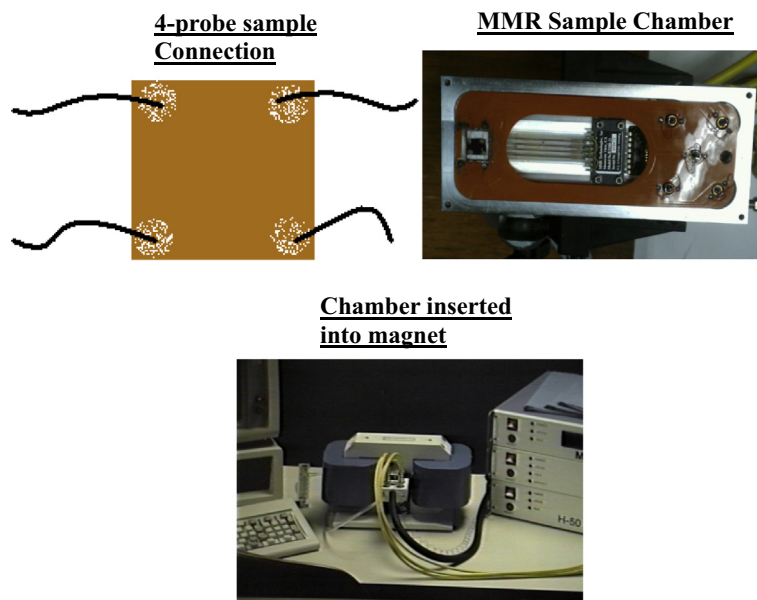


Fig. 3. The in-plane electrical conductivity (Van der Pauw) and Hall Effect measurement system.

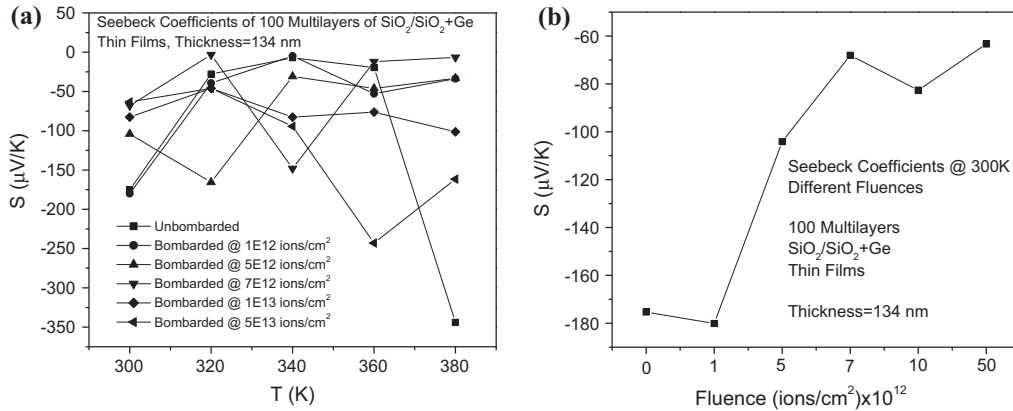


Fig. 4. Fluence dependence of the cross- plane Seebeck coefficient (a) at the different temperatures and (b) at room temperature.

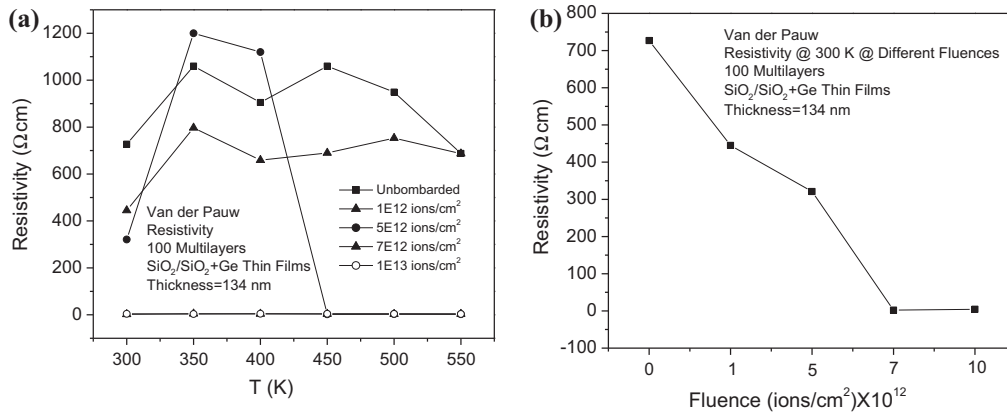


Fig. 5. Fluence dependence of the van der Pauw resistivity measurements (a) at the different temperatures and (b) at room temperature.

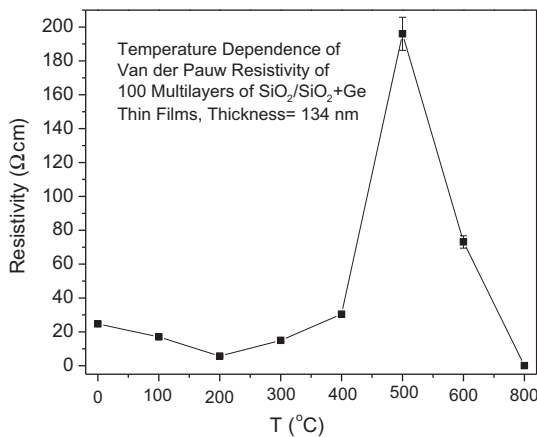


Fig. 6. Temperature annealing dependence of the van der Pauw resistivity measurements.

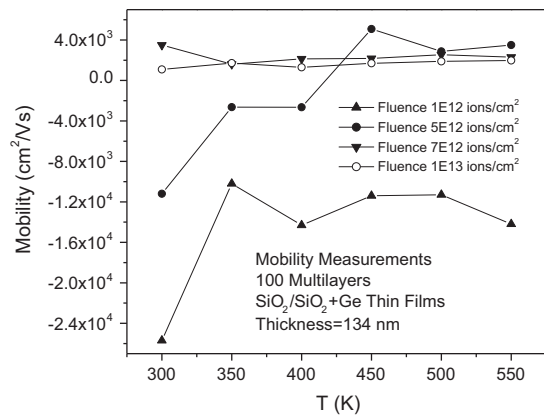


Fig. 7. Fluence dependence of mobility measurements at the different temperatures.

affects providing additional ways to enhance energy conversion efficiencies in nano-structured materials [9]. Much effort has been carried out to improve the performance of thermoelectric films by increasing the electrical conductivity and the Seebeck coefficient. However, they are difficult to improve because the elements in  $ZT$  are not independent [10]. Many relevant interdisciplinary areas

of physics, chemistry, and material sciences are developing rapidly including ion induced modifications of solids, thin films, surfaces and interfaces to improve the properties of solids up to a shallow depth [11]. We have been working on different thermoelectric systems [12–17]. Some of them were on  $\text{SiO}_2/\text{SiO}_2 + \text{Ge}$  thin film systems [9,18]. We have obtained remarkable results on those

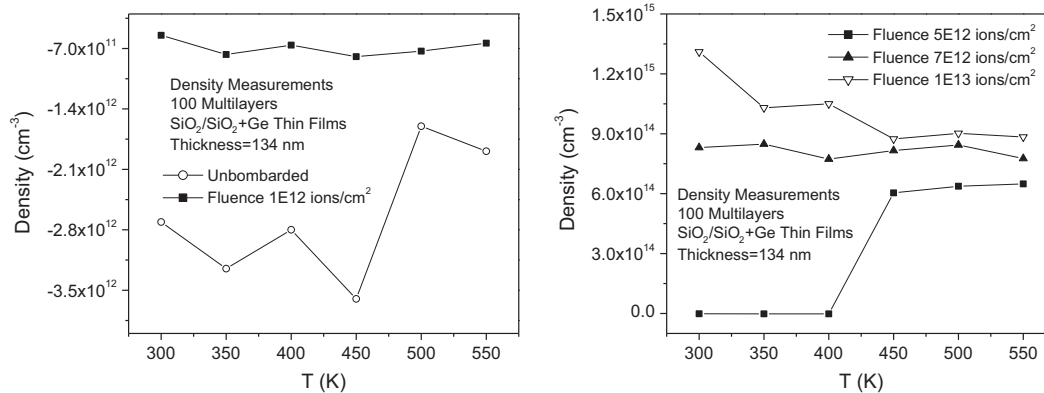


Fig. 8. Fluence dependence of density (carrier concentration) measurements at the different temperatures.

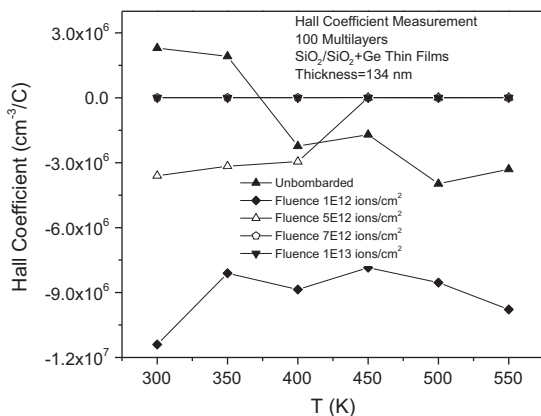


Fig. 9. Fluence dependence of Hall Effect coefficient measurements at the different temperatures.

studies from thermoelectrical and optical respects. In this study we report on the growth of  $\text{SiO}_2/\text{SiO}_2 + \text{Ge}$  multilayer superlattice thin film systems prepared by magnetron DC/RF sputtering; high energy Si ion bombardment of the thin films for increasing the cross plane electrical conductivity and the cross plane Seebeck

coefficients due to the nano-clusters effect during the MeV Si ion bombardment; van der Pauw resistivity, mobility, density (carrier concentration), Hall Effect coefficient, Raman, Fluorescence, Photoluminescence, Atomic Force Microscopy (AFM) and Impedance analysis measurements.

## 2. Experimental

We have deposited the thin films with 100 alternating layers of  $\text{SiO}_2/\text{SiO}_2 + \text{Ge}$  nano-layers on silicon (Si) and fused silica (suprasil) substrates by magnetron DC/RF sputtering as the deposition geometry was shown in Fig. 1. The multilayer thin films were sequentially deposited to have a periodic structure consisting of alternating  $\text{SiO}_2$  and  $\text{SiO}_2 + \text{Ge}$  layers. These thin films form a periodic quantum well structure consisting of 100 alternating layers of total thickness of 134 nm. The DC gun was used to sputter Ge material while RF gun was used to sputter  $\text{SiO}_2$ . Ar gas was used to form plasma in the DC/RF sputtering chamber during the deposition. The chamber was pumped down to about  $1 \times 10^{-5}$  Torr. The deposition was performed when the pressure was about  $3 \times 10^{-3}$  Torr. The substrates were mounted on the substrate holder and rotated during the whole deposition process. The growth rate was monitored by an INFICON Quartz Crystal Microbalance (QCM). In order to form nano-structures (nano dots and/or nano

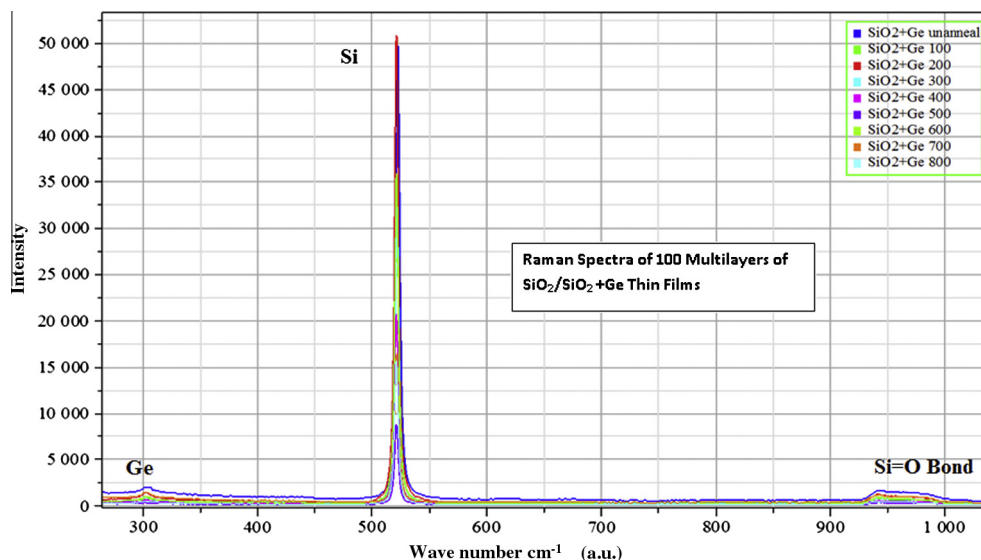
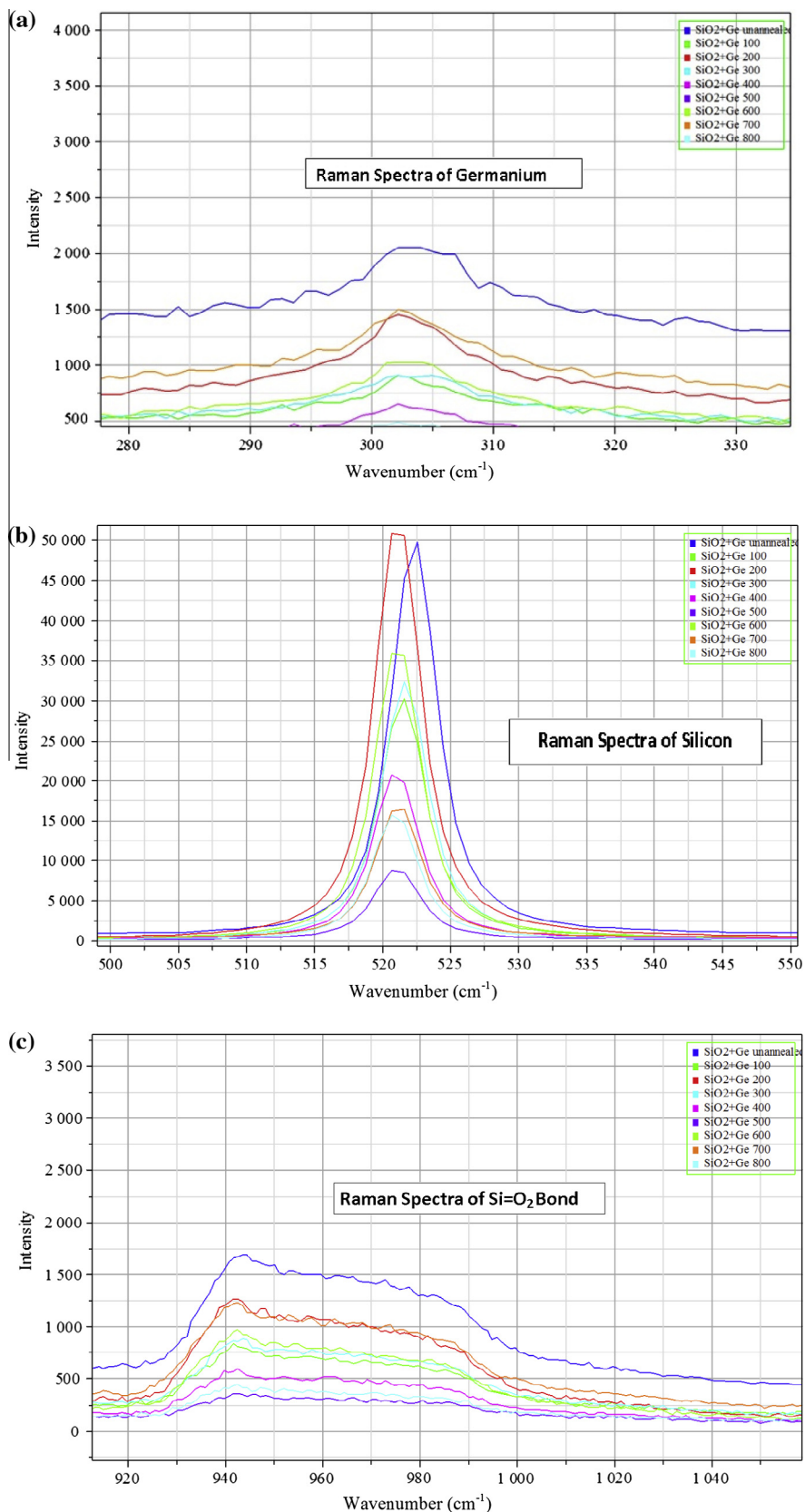


Fig. 10. Temperature annealing dependence of Raman spectra at the different temperatures.



**Fig. 11.** Temperature annealing dependence of Raman spectra at the different temperatures for (a) Germanium, (b) Silicon, and (c)  $\text{Si}=\text{O}_2$  bonds.

clusters) in the multilayers, 5 MeV Si ion bombardments were performed with the Pelletron ion beam accelerator at the Alabama A&M University Materials Research Laboratory (AAMU-MRL). The

energy of the bombarding Si ions was chosen using the Stopping Range Ions in Matter (SRIM) simulation software. SRIM shows that 5 MeV Si ions pass through the multilayer thin films and terminate



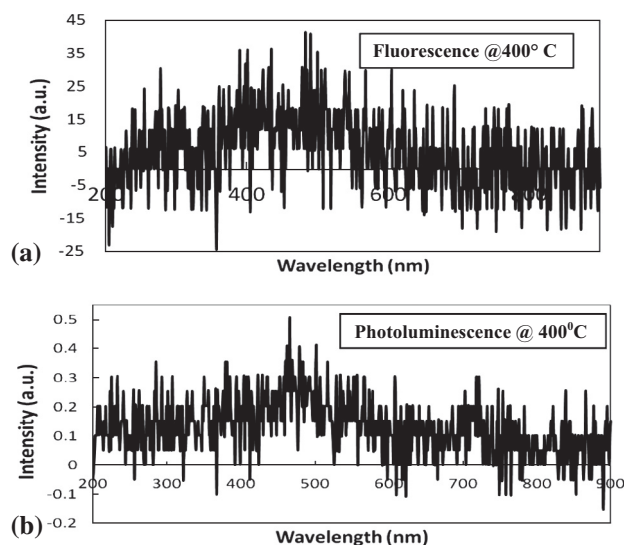


Fig. 12. (a) Fluorescence spectrum and (b) Photoluminescence spectrum at 400 °C.

deep in the substrate. The fluences used for the bombardment were selected between  $1 \times 10^{12}$  ions/cm<sup>2</sup> and  $1 \times 10^{12}$  ions/cm<sup>2</sup>. Rutherford Backscattering Spectrometry (RBS) was performed using 2.1 MeV He<sup>+</sup> ions with particle detector placed at 170° from the incident beam, in order to determine elemental abundances [19–21]. Cross plane Seebeck coefficients, in-plane electrical conductivity, density (carrier concentration), mobility and Hall Effect coefficients measurements as a function of temperature under the different applied fluences were measured by MMR van der Pauw and Hall Effect measurement system. In addition to the thermoelectrical properties, Raman, Fluorescence, Photoluminescence, AFM and Impedance measurements were also performed for this study. Thermoelectric measurement techniques were selected to show how this material system will be useful in future researches as thermoelectric generators to convert to waste heat to electrical energy or as thermoelectric cooling devices for cooling of many microelectronic devices using Seebeck, van der Pauw, Hall Effect, mobility, and density (carrier concentration) measurements. Optical measurement techniques were used to detect nano-clustering in the multilayer films like Raman spectroscopy; to show the transparency due to nano-clustering contribution on the fused silica samples like Fluorescence and Photoluminescence spectroscopies. AFM was used to see the effects of the thermal annealing on the surface of multilayer thin films. The LF4192A (Hewlett-Packard) Impedance Analyzer was used in understanding the ac “small-signal” electrical behavior of the entire thermoelectric device. This is a two-terminal measurement that yields underlying operative mechanism via an equivalent circuit model.

### 3. Results and discussion

The geometry for the Seebeck coefficient measurement was given in Fig. 2 and the in-plane electrical conductivity (Van der Pauw) and Hall Effect measurement system is given in Fig. 3.

The van der Pauw and Hall Effect system is the same system. When the thin film sample was located on the van der Pauw measurement stage, van der Pauw resistivity measurement, Hall Effect measurement under the applied magnetic field, density (carrier concentration), and mobility measurements have been performed using the same stage and the same sample. The measurement software gives results of van der Pauw resistivity, Hall Effect coefficient, mobility, density on the same screen.

Fig. 4 shows the fluence dependence of the cross-plane Seebeck coefficients (a) at different temperatures, (b) at room temperature. The original Seebeck coefficients are negative and we have negative thermo-power since electrons are the main charge carriers. As seen from Fig. 4, the results could be interpreted from two perspectives: (a) Fig. 4(a) shows the fluence dependence of Seebeck variation under the different temperatures, and (b) Fig. 4(b) shows the Seebeck coefficients determined at the room temperature at the different fluences. The virgin sample (unbombarded) has the Seebeck coefficient of  $-175.33 \mu\text{V/K}$  at room temperature and this value increased to  $-344.02 \mu\text{V/K}$  at 380 K. Seebeck coefficients showed increment and decrement at the applied fluences. Since higher Seebeck coefficient is needed for the high efficient thermoelectric devices, suitable fluences and temperatures should be selected and used.

Fig. 5 shows the fluence dependence of the van der Pauw resistivity measurements (a) at the different temperatures between 300 K and 550 K, and (b) at room temperature. As seen from Fig. 5, the in-plane electrical resistivity values show both increment and decrement at the applied different fluences under the temperature change. Fig. 5(b) shows exactly what is needed for building high efficiency thermoelectric devices since the electrical resistivity values started to decrease at the different applied fluences at room temperature until the last fluence was reached. The decrease in the resistivity for the semiconductor thin films depending on the increased temperature is one of the expected things in the semiconductor and thermoelectric material systems.

Fig. 6 shows the annealing temperature dependence of the van der Pauw resistivity measurements. Fig. 6 tells us that thermal annealing of the thin film systems did not bring benefits since the electrical resistivity values increased with respect to the starting value at the room temperature, even though the resistivity values are expected to be smaller. For the future effective studies, we will focus on more detailed temperature optimization studies using more detailed temperature interval during the annealing procedure for the characterization of the fabricated thin film systems sensitively to see accurate effects on the resistivity.

Fig. 7 shows the fluence dependence of mobility measurements at the different temperatures between 300 K and 550 K. The mobility values started to shift from negative values to positive values under the different high energy fluences and temperatures. This suggests that the thin film system shows a transition from quasi-n type structure to the quasi p-type semiconductor structure. This could be explained as the effect of the positive ion increase due to the ion bombardment of Si ions. As seen from Fig. 7, the shift of the density from the negative values could arise from the positive ion concentration increase due to high energy Si ion bombardments at the higher fluences.

Fig. 8 shows the fluence dependence of density (carrier concentration) measurements at the different temperatures. Similar effects have been seen in the mobility values. The density values started to shift from negative direction to positive direction as if the sample systems started to transit from quasi-n type semiconductor structure to the quasi-p type semiconductor structure due to the increase in the positive numbers of charge carriers.

Fig. 9 shows the fluence dependence of Hall Effect coefficient measurements at the different temperatures between 300 K and 550 K. While the thin films systems were bombarded with the increasing fluence, the Hall Effect coefficients started to shift in the negative y-axis and, then they changed their directions back to the positive y-axis as if the ion bombardment changed their Hall Effect coefficients from n-type structure to the p-type structure and coming back to n-type structure with increasing energy fluences.

Fig. 10 shows the annealing temperature dependence of Raman spectra. The Raman spectra may be seen in more details in Fig. 11

at various temperatures for (a) Germanium, (b) Silicon, (c) Si = O<sub>2</sub> bonds. Since the amount of the Ge in the thin films depends on the annealing temperature, the intensity of the peaks for the elements in the thin film systems decreases while the annealing temperature is increasing. In other words, the suitable annealing temperature causes melting and diffusing of Ge atoms through the multilayer thin films. If the annealing temperatures increase too much, the amount of Ge atoms leave the thin film systems due to evaporation.

Fig. 12 shows (a) Fluorescence spectrum and (b) Photoluminescence spectrum at 400 °C. Both spectra gave peaks at 500 nm showing the transparency due to Ge nano-clustering contribution on the fused silica samples. In other words, suitable annealing temperature causes Ge nano-clustering formation through the multilayer thin films, thus the optical properties may improve through nano-clustering centers in the multilayers. More detailed studies are planned on the optical properties of these structures.

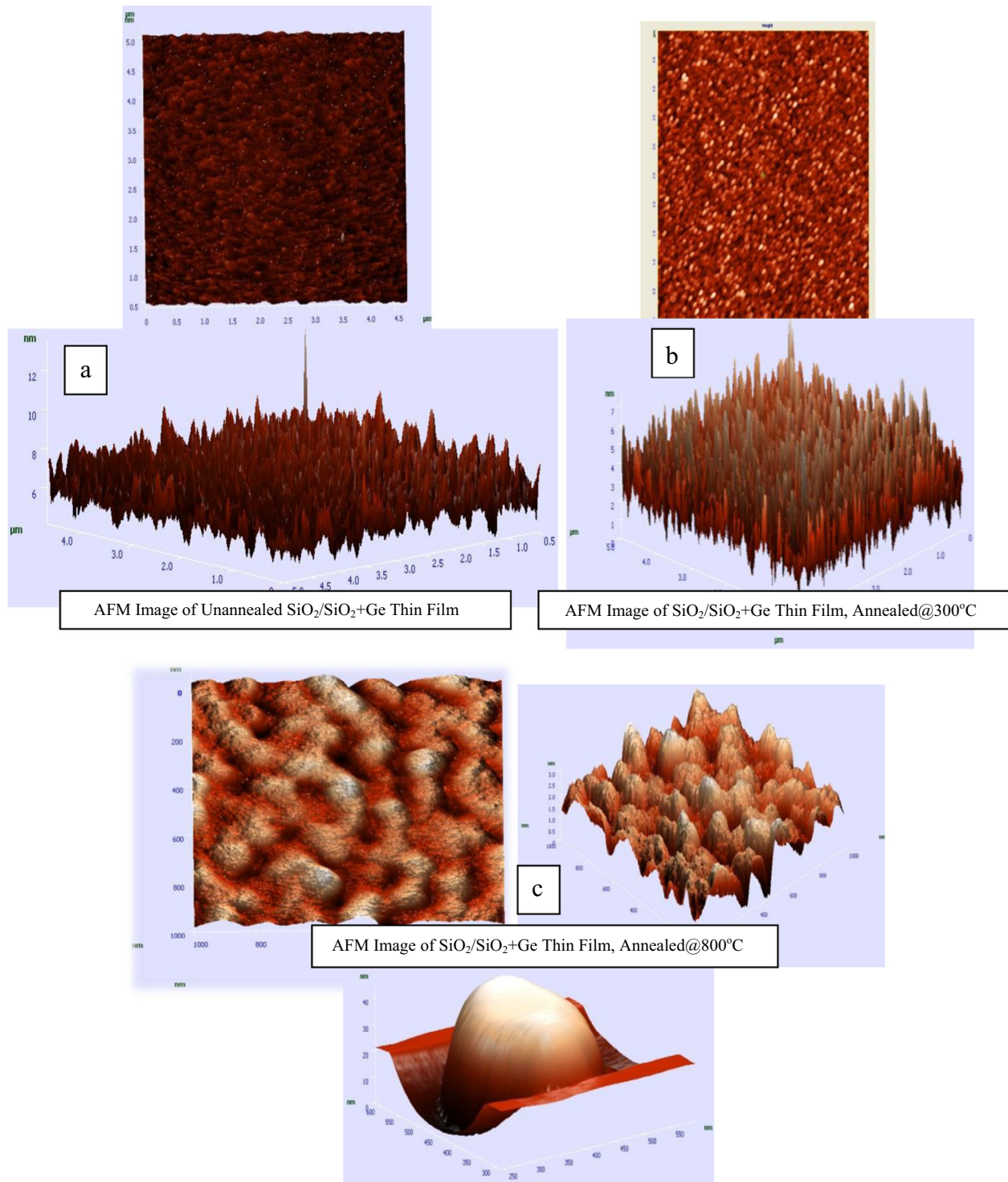
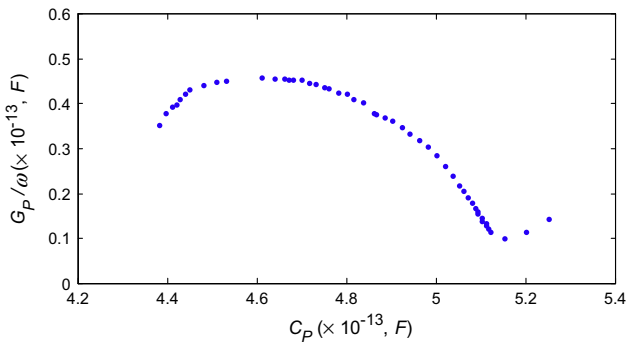


Fig. 13. AFM images of (a) unannealed, (b) annealed at 300 °C, and (c) annealed at 800 °C.



**Fig. 14.** The complex capacitance ( $C^* = C' - j C'' = C_p - j G_p/\omega$ ) plot of the unbombarded 100-layered stack comprising of repeated Si + Ge/SiO<sub>2</sub> monolayer layer on to SiO<sub>2</sub> layer for the frequency range 20 Hz – 13 MHz.

Fig. 13 shows AFM images of (a) unannealed, (b) annealed at 300 °C, and (c) annealed at 800 °C. When the sample was annealed at 300 °C, the surface suggests nanowire growth perpendicular to the film surface. One of the type of the nanowire growth is initiated with a metal catalyst and causing a nanowire growth under this metal head [22]. This could be found easily by searching in the internet. Here, Ge atoms behave like a metal catalyst to cause an initiation of the nanowire growth on the surface with the contribution of Si, O<sub>2</sub> and Ge elements. After the sample was annealed at 800 °C, the surface nanowires could come together and show “dome-type” structures. If suitable temperature could be selected, the nano-clustering could take place in the multilayer structures and that could increase the Seebeck coefficient and the electrical conductivity, thus increasing the efficiency of the thermoelectric devices.

Fig. 14 shows the complex capacitance ( $C^* = C' - j C'' = C_p - j G_p/\omega$ ) plot of the unbombarded 100-layered stack comprising repeated Si + Ge/SiO<sub>2</sub> monolayer layer on to SiO<sub>2</sub> layer, for the frequency range 20 Hz–13 MHz. The *ac* small-signal electrical data were acquired using HP4192A Impedance Analyzer for the unbombarded 100-layered stack comprising repeated Si + Ge/SiO<sub>2</sub> monolayer layer on to SiO<sub>2</sub> layer for the frequency range 20 Hz–13 MHz. These data are analyzed via complex plane formalisms. Skewed semicircular response (via equal grid scaling) is observed in the complex capacitance ( $C^* = C' - j C'' = C_p - j G_p/\omega$ ) plane. The loci obtained in the  $C^*$ -plane for these data indicate non-Debye type relaxation displaying the presence of the depression parameter. The skewed semicircular behavior also shows the contribution of the shunt *dc* resistance (conductance) at the low frequency end. The semicircular relaxation yields R–C (resistance–capacitance) series equivalent circuit with a shunt resistance. However, in the low frequency domain the entire stack shows as a non-leaky capacitor. At increasing frequencies the same capacitor turned to R–C circuit having a shunt with it. Also the intercept on the left side of the semicircle provides capacitance in parallel with the entire equivalent circuit combination [23–25].

#### 4. Conclusion

We have grown 100 periodic nano-layers of SiO<sub>2</sub>/SiO<sub>2</sub> + Ge superlattice thin films on the silicon and fused silica substrates (suprasil) at the total thickness of 134 nm using magnetron DC/RF sputtering. The multilayer thin films were sequentially deposited to have a periodic structure consisting of alternating SiO<sub>2</sub> and SiO<sub>2</sub> + Ge layers. The deposited multilayer films have alternating layers of about 1.3 nm thick each. Some thermoelectrical and

optical properties showed some meaningful results depending on the modification of the thin film systems by high energy Si ion bombardments to cause formation of nano-dots and/or clusters in the multilayer structures. We are planning to continue to work on these systems under different modified conditions since we have reached also very meaningful data [9,18] and high figure of merit in our previous studies [9].

#### Acknowledgements

Research was sponsored by the Materials Research Laboratory (AAMU-MRL), National Science Foundation under NSF-EPSCOR R-II-3 Grant No. EPS-1158862, DOD under Nanotechnology Infrastructure Development for Education and Research through the Army Research Office # W911 NF-08-1-0425, and DOD Army Research Office # W911 NF-12-1-0063 and National Nuclear Security Admin (DOE/NNSA/MB-40) with Grant# DE-NA0001896, NSF-REU with Award#1156137.

#### References

- [1] Sahin Ahmet Z, Yilbas Bekir S. The thermoelement as thermoelectric power generator: effect of leg geometry on the efficiency and power generation. *Energy Convers Manage* 2013;65:26–32.
- [2] Patyk Andreas. Thermoelectric generators for efficiency improvement of power generation by motor generators – environmental and economic perspectives. *Appl Energy* 2013;102:1448–57.
- [3] Fan Ping, Li Ying-zhen, Zheng Zhuang-hao, Lin Qing-yun, Luo Jing-ting, Liang Guang-xing, et al. Thermoelectric properties optimization of Al-doped ZnO thin films prepared by reactive sputtering Zn–Al alloy target. *Appl Surf Sci* 2013;284:145–9.
- [4] Bhaskar Ankam, Liu Chia-Jyi, Yuan JJ, Chang Ching-Lin. Thermoelectric properties of n-type Ca<sub>1-x</sub>Bi<sub>x</sub>Mn<sub>1-y</sub>SiO<sub>2-d</sub> ( $x = y = 0.00, 0.02, 0.03, 0.04$ , and 0.05) system. *J Alloys Comp* 2013;552:236–9.
- [5] Jang Jiin-Yuh, Tsai Ying-Chi. Optimization of thermoelectric generator module spacing and spreader thickness used in a waste heat recovery system. *Appl Therm Eng* 2013;51:677–89.
- [6] Guo Juncheng, Zhang Xiuqin, Guozhen Su, Chen Jincan. The performance analysis of a micro/nanoscaled quantum heat engine. *Physica A* 2012;391:6432–9.
- [7] Zhao-kun Cai, Ping Fan, Zhuang-hao Zheng, Peng-juan Liu, Tian-bao Chen, Xing-min Cai, et al. Thermoelectric properties and micro-structure characteristics of annealed N-type bismuth telluride thin film. *Appl Surface Sci* 2013;280:225–8.
- [8] Hmood A, Kadhim A, Abu Hassan H. Fabrication and characterization of Pb<sub>1-x</sub>Yb<sub>x</sub>Te-based alloy thin-film thermoelectric generators grown by thermal evaporation technique. *Mater Sci Semicond Process* 2013;16:612–8.
- [9] Budak S, Parker R, Smith C, Muntele C, Heidary K, Johnson RB, Ila D. Superlattice multi-nanolayered thin films of SiO<sub>2</sub>/SiO<sub>2</sub>+Ge for thermoelectric device applications. *J Intell Mater Syst Struct* 2013;24(11):1357–64.
- [10] Lee Hee-Jung, Park Hyun Sung, Han Seungwoo, Kim Jung Yup. Thermoelectric properties of n-type Bi–Te thin films with deposition conditions using RF magnetron co-sputtering. *Thermochim Acta* 2012;542:57–61.
- [11] Jain IP, Agarwal Garima. Ion beam induced surface and interface engineering. *Surf Sci Rep* 2011;66:77–172.
- [12] Budak S, Smith C, Muntele C, Chhay B, Heidary K, Johnson RB, Ila D. Thermoelectric properties of SiO<sub>2</sub>/SiO<sub>2</sub> + CoSb multi-nanolayered thin films modified by MeV Si ions. *J Intell Mater Syst Struct* 2013;24(11):1350–6.
- [13] Budak S, Smith C, Chacha J, Muntele C, Ila D. Characterization of gold nanodots arrangements in SiO<sub>2</sub>/SiO<sub>2</sub>+Au nanostructured metamaterials. *Radiat Eff Defects Solids* 2012;167:607–11.
- [14] Budak S, Chacha J, Smith C, Pugh M, Heidary K, Johnson RB, et al. Effects of MeV Si ion bombardment on the thermoelectric generator from SiO<sub>2</sub>/SiO<sub>2</sub> + Cu and SiO<sub>2</sub>/SiO<sub>2</sub> + Au nanolayered multilayer films. *Nucl Instr Methods B* 2011;269:3204–8.
- [15] Budak S, Guner S, Minamisawa RA, Ila D. MeV Si ions bombardment effects on the thermoelectric properties of nano-layers of nanoclusters of Ag in SiO<sub>2</sub> host. *Surf Coat Technol* 2009;203:2479–81.
- [16] Budak S, Guner S, Smith C, Minamisawa RA, Zheng B, Muntele C, et al. Surface modification of Si/Ge multi-layers by MeV Si ion bombardment. *Surf Coat Technol* 2009;203:2418–21.
- [17] Zheng B, Budak S, Zimmerman RL, Muntele C, Chhay B, Ila D. Effect of layer thickness on thermoelectric properties of multilayered Si<sub>1-x</sub>Ge<sub>x</sub>/Si after bombardment by 5 MeV Si ions. *Surf Coat Technol* 2007;201:8531–3.
- [18] Budak S, Smith C, Pugh M, Heidary K, Colon T, Johnson RB, Ila D. MeV Si ions bombardment effects on thermoelectric properties of thermoelectric of SiO<sub>2</sub>/SiO<sub>2</sub>+Ge Nanolayers. *Radiat Phys Chem* 2012;81:410–3.
- [19] Chacha J, Budak S, Smith C, McElhaney D, Pugh M, Ogbara K, et al. Thermoelectric properties of SiO<sub>2</sub>/SiO<sub>2</sub>+Au nano-layered superlattices modified by MeV Si ions beam. *AIP Conf Proc* 2011;1336:257–9.



- [20] Ziegler JF, Biersack JP, Littmark U. The stopping range of ions in solids. New York: Pergamon Press; 1985.
- [21] Chu WK, Mayer JW, Nicolet M-A. Backscattering spectrometry. New York: Academic Press; 1978.
- [22] Budak S, Miao GX, Ozdemir M, Chetry KB, Gupta Arunava. Growth and characterization of single crystalline tin oxide (SnO<sub>2</sub>) nanowires on different substrates. J Cryst Growth 2006;291:405.
- [23] Alim MA. Electrical characterization of engineering materials. Acta Passiva Electron Compon 1996;19:139–69.
- [24] Wang CC, Chen WH, Akbar SA, Alim MA. High-temperature a.c. electrical behaviour of polycrystalline calcium zirconate. J Mater Sci 1997;32:2305–12.
- [25] Azad AM, Shyan LLW, Alim MA. Electrical characterization of the solid-state reaction derived CaSnO<sub>3</sub>. J Mater Sci 1999;34:3375–96.